*mathematics*

MDPI

*Article*

# On the Impact of Quarantine Policies and Recurrence Rate in Epidemic Spreading Using a Spatial Agent-Based Model

**Alexandru Topîrceanu**

Department of Computer and Information Technology, Politehnica University Timişoara, 300006 Timisoara, Romania; alext@cs.upt.ro

**Abstract:** Pandemic outbreaks often determine swift global reaction, proven by for example the more recent COVID-19, H1N1, Ebola, or SARS outbreaks. Therefore, policy makers now rely more than ever on computational tools to establish various protection policies, including contact tracing, quarantine, regional or national lockdowns, and vaccination strategies. In support of this, we introduce a novel agent-based simulation framework based on: (i) unique mobility patterns for agents between their home location and a point of interest, and (ii) the augmented SICARQD epidemic model. Our numerical simulation results provide a qualitative assessment of how quarantine policies and the patient recurrence rate impact the society in terms of the infected population ratio. We investigate three possible quarantine policies (proactive, reactive, and no quarantine), a variable quarantine restrictiveness (0–100%), respectively, and three recurrence scenarios (short, long, and no recurrence). Overall, our results show that the proactive quarantine in correlation to a higher quarantine ratio (i.e., stricter quarantine policy) triggers a phase transition reducing the total infected population by over 90% compared to the reactive quarantine. The timing of imposing quarantine is also paramount, as a proactive quarantine policy can reduce the peak infected ratio by over $\times 2$ times compared to a reactive quarantine, and by over $\times 3$ times compared to no quarantine. Our framework can also reproduce the impactful subsequent epidemic waves, as observed during the COVID-19 pandemic, according to the adopted recurrence scenario. The suggested solution against residual infection hotspots is mobility reduction and proactive quarantine policies. In the end, we propose several nonpharmaceutical guidelines with direct applicability by global policy makers.

**Keywords:** agent-based model; epidemic model; computational epidemics; epidemic control policies; nonpharmaceutical interventions

**MSC:** 93A16; 91D10; 92D30; 68T09



**Citation:** Topirceanu, A. On the Impact of Quarantine Policies and Recurrence Rate in Epidemic Spreading Using a Spatial Agent-Based Model. *Mathematics* **2023**, *11*, 1336. https://doi.org/10.3390/math11061336

Academic Editors: Cristiano Maria Verrelli and Fabio Della Rossa

Received: 15 January 2023
Revised: 23 February 2023
Accepted: 8 March 2023
Published: 9 March 2023



## 1. Introduction

Understanding the dynamics of pandemics (e.g., COVID-19, H1N1, Ebola, SARS, etc.) is an ongoing multidisciplinary scientific challenge and a public health priority for many governments around the world [1–3]. The conventional epidemiological approach, or the analytic approach, offers solutions by employing compartmental models that divide the population into groups based on economics, demographics, and other characteristics. It has been shown that even though compartmental models lack the complexity of individuals behavior, they are exceedingly successful in informing and developing public health policies [4–6].

The analytic approach involves gradually changing one variable at a time to deduce general laws that allow for predictions about the system's properties under varying conditions, which hold true in homogeneous systems consisting of similar elements with weak interactions between them [7]. In addition, systems consisting of a diversity of elements linked together by strong interactions employ the newer paradigm of complex systems. These complex systems methods aim to examine the system as a whole, taking into account

its complexity and inherent dynamics. Through discrete event computer simulation of the system, one can observe the effects of various interactions between its elements in real time. Through the study of behavior, rules that can alter the system can eventually be determined [7,8].

Over the last decade, following the paradigm of complex systems, agent-based modeling (ABM) approaches have been developed to simulate epidemic outbreaks that enable embedding the behavior of individuals and their inherent stochasticity by characterizing every individual as a (simplified) social agent in an agent population. Each social agent is characterized by several parameters considered relevant for the viral spreading process, e.g., mobility patterns, physical social networking, social, minority, and economical status, or age. For example, during the debut of the COVID-19 pandemic, ABM was successfully used in exchange for simpler compartmental models, like SIR, SIS [9,10]. Later approaches also focused on developing epidemic models which consider more specific patient states like quarantined, infected and aware, vaccinated, asymptomatic, etc. One of these early compartmental models is SICARS, which was introduced by the authors in 2020 [11], and which we aim to further develop in this study.

In the face of existing challenges, we enumerate several state-of-the-art impactful studies that mainly improve mass action models into tools applicable to analyzing large epidemics [4,5,12–14]. Nevertheless, the underlying epidemic models used by the majority of papers are limiting (e.g., SI, SIS, SIR, SEIR, SIRS), as they are unable to implement the effects gradual quarantining, variable recurrence rates, and vaccination policies. Furthermore, their simplification of spatial and social organization lacks the complexity of population organization [15]. Therefore, the numerical results of such models can lead to over-/underestimations of the impact of an epidemic [6,14].

To address these limitations, our main motivation is to investigate the impact of two important nonpharmaceutical interventions, i.e., quarantine timing and strength of isolation policies, corroborated with variable patient recurrence rates based on ABM combined with an augmented epidemic model. Thus, our research aims to answer the following questions:

1. How does the *timing of quarantine* affect the maximum and total estimated ratios of the infected population?
2. How does the *recurrence rate* (i.e., duration of natural immunity) affect the ratio of infected population in time?
3. How does the *ratio of quarantined* infected population (i.e., isolation policy strength) affect the dynamics of an epidemic?
4. How does every control measure compare to the baseline (i.e., no action whatsoever) in terms of the epidemic outcome?

Answering these questions can lead us toward developing a set of qualitative "guidelines" for effective epidemic control with direct social impact, as well as impact in interdisciplinary applications, like epidemiology, modeling and simulation, and healthcare.

Closely related work on ABM for epidemic control is limited in the sense that most studies are either confined to specific geographical regions, or make use of epidemic models which are not aimed at studying control policies. For example, authors Hoertel et al. define an ABM with embedded data for France [16]; similarly, Datta et al. embed their ABM with data specific to the state of New York [17]. Hinch et al. provide a more robust ABM, called OpenABM-Covid19, tuned for the UK [10], but one that can be adjusted for other countries; however, their model is specifically a "flattening the curve" solution that does not consider reinfection and possible subsequent infection waves. In contrast, our simulation framework uses an epidemic model that permits, under the right parameters, epidemic waves to recur. In another study, authors Frias-Martinez et al. [18] propose an ABM aimed at H1N1 that does not consider quarantine policies. The work of Alzu'bi et al. is similar in terms of methodology, but aims towards a different research goal, without discussing the implications of quarantine policies [19].

Taken together, our main contribution is studying the effect of control procedures—through quarantine timing and strength, in the wake of different recurrence rates—to

contain the epidemiological effect over closed populations. Our ABM offers an original contribution in regard to agent mobility patterns based on points-of-interest (POIs), which have been proven to represent infection hotspots in densely populated areas [20–22].

The rest of the paper is structured in the following order: the Section 2 section presents the epidemic model, the COVID-19 parameter settings, and the agent-based spatial model used in our simulations; the Section 3 section summarizes the simulation output and details the analysis over each experiment; the Section 4 section outlines a meta-analysis to understand the impact of each ABM parameter and presents conclusions from the experiments; the Section 5 outline the main results and enumerate the contributions of this work, including future directions for the presented research.

## 2. Materials and Methods

The study presents a multi-compartment model that tracks the spread of an epidemic at a macro-level within a community with a variable micro-structure, which is based on the local movements of agents. By considering the infectious status of agents in different compartments and controlling their movements, the model is able to accurately simulate the real-world mobility of the population and the progression of the outbreak.

We further detail the reasoning and methodology for developing the SICARQD epidemic model and the agent-based model used to simulate the target population. Given the multitude of possible parameters in an epidemic model as well as an ABM, we consider incorporating an intuitive set of rules for the individuals' mobility patterns and their spatial distribution. Specifically, to achieve our research goals, we augment the previously developed SICARS epidemic model [11] into the newly proposed SICARQD model to allow the evaluation of quarantine policies.

As a note, SICARS is a generalization of the popular SIR model [23,24], which we explicitly aimed at the analysis of isolation strategies that were relevant to the COVID-19 outbreak. To this end, SICARS defines five possible states for an individual: *susceptible* $S$, *incubating* $I$, *contagious* $C$, *aware* $A$, and *removed* $R$, with the note that $R$ merges both *recovered* and *dead* compartments. Nevertheless, SICARS was developed as an *edge-removal model* to be used in a complex network context, rather than as an ABM. Further, our SICARQD epidemic model does not consider asymptomatic cases, which can occur during SARS-CoV-2 infection, so the estimated number of infected agents and the impact of the discussed quarantine policies can vary based on the actual real-world setting.

In addition, we make use of discrete event simulation which is a recognized option in the computational epidemiology literature for modeling high complexity and detail, where complexity is specifically the result of multiple random processes and the inherent structure of the system [25].

### 2.1. The SICARQD Epidemic Model

The proposed epidemic model is summarized in Figure 1 which defines the seven possible states and the particular transition rates. An agent can be in one of the following states: *susceptible* $S$, *incubating* $I$, *contagious* $C$, *aware* $A$, *quarantined* $Q$, *recovered* $R$, or *dead* $D$. The transition $S \rightarrow I \rightarrow C \rightarrow A \rightarrow R$ is determined by the following infection and recovery rates:

- $\lambda_{inf}$: rate for *susceptible* agents to become infected in the vicinity of an infectious agent (which is in the $C$ or $A$ states). An agent in the $I$ state does not infect other agents.
- $\lambda_{ctg}$: rate of becoming contagious $C$ after a specific period (depending on the modeled virus). In this state, an agent does not know that it is infected, yet it infects others.
- $\lambda_{awr}$: rate of becoming aware $A$ after a specific period. In this state, an agent knows that it is infected, and it infects other agents in its vicinity.
- $\lambda_{rec}$: recovery rate after a specific infectious period. The transition determines whether an agent has fully recovered, becoming temporarily immune ($R$), or whether the agent has died ($D$) based on the death ratio $r_{death}$. Recovered agents $R$ may not be infected.
- $\lambda_{rcr}$: recurrence rate to *susceptible* after a specific period of recovery from infection.

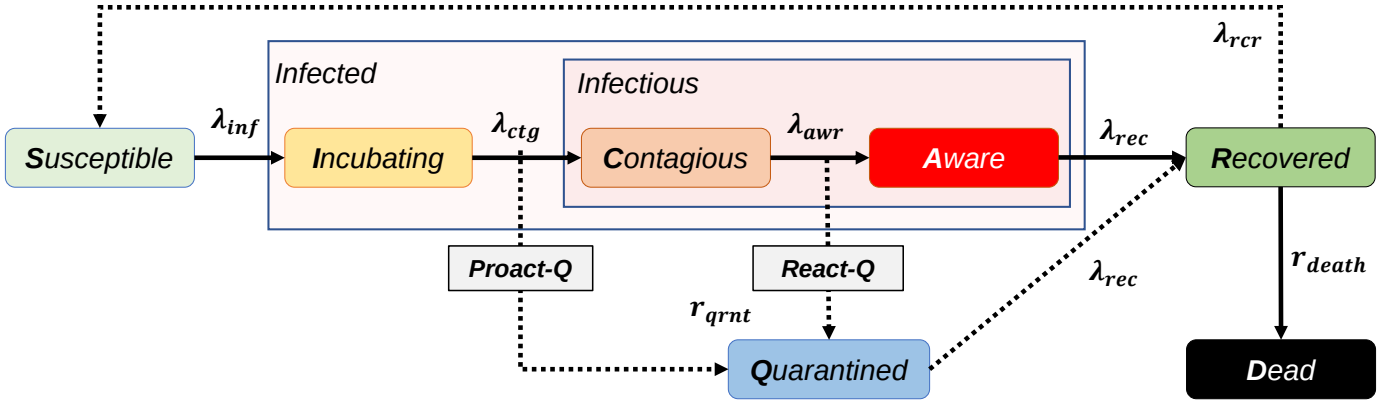


**Figure 1.** The states and parameters that define the SICARQD epidemic model. By splitting the infectious stage into two states—*contagious* and *aware*—our model offers the capability of implementing so-called proactive or reactive quarantine policies. The rates specific to transitions between infectious states are denoted with $\lambda$, and the ratios of quarantined and dead patients are denoted with $r$.

Furthermore, the transition to the quarantined state $Q$ may occur when an agent moves to the contagious state $C$ or to the aware state $A$. The number of quarantined agents corresponds to $r_{qrnt}$, which represents the ratio of infected patients that can be isolated from others, further removing their infectious capacity. As suggested by the dashed arrows in Figure 1, we implement three possible quarantine policies:

1. Proactive quarantine (**proact-Q**), which means that a proportion of agents will be quarantined immediately as they transit to become contagious $C$. This policy is the most expensive in the real world and involves contract tracing and intensive population-wide testing; also, this policy can prove to be the most effective way to mitigate infectious spreading.
2. Reactive quarantine (**react-Q**), which means that a proportion of agents will be quarantined right when they transit to become aware $A$. This policy is less costly, but requires population-wide testing and population awareness such that symptomatic individuals will auto-quarantine.
3. No quarantine (**no-Q**), which means that state $Q$ is never used and that all infected agents remain active in the population. This is the baseline policy used for comparison.

Based on the recurrence rate $\lambda_{rcr}$, we determine whether the recovered state $R$ is a final state or not. Consequently, we implement three recurrence scenarios:

1. Short recurrence scenario (**short-R**), corresponding to an average, normally distributed, 3 month immunity period.
2. Long recurrence scenario (**long-R**), corresponding to an average, normally distributed, 12 month immunity period.
3. Never-recurrence scenario (**never-R**), corresponding to a $\lambda_{rcr} = 0$, thus granting permanent immunity to all agents that reach the recovered state. This scenario is less realistic in the case of most infectious diseases, but serves as a baseline for comparison.

### *2.2. Literature Review for COVID-19 Infectious Parameters*

Although our SICARQD model may be parameterized for other viruses, including future viruses, in this paper, we focus on customizing the experimental setup for the SARS-CoV-2 virus responsible for the COVID-19 pandemic.

Consequently, Table 1 details the settings for each model parameter, as supported by recent COVID-19 studies. All parameters correspond to those illustrated in Figure 1 and are based on an extensive review of the literature. In general, where we found several estimations, we picked either the worst case (see superscript [1]), or a rounded average value (without superscript). The last two parameters in Table 1 (see superscript [2]) are being investigated in our paper, so they take values in a wider range.

More precisely, we set the recurrence rates for recovered individuals to be normally distributed around 3 months for short-R and 12 months for long-R, respectively, as supported by recent estimates of COVID-19 immunity found in the recent literature: 3 months [26], 4–5 months [27], 6 months [28], and up to 1 year [29]. We also assign the quarantine ratio with values from 0 to 1, with a step of 0.1, that is, $r_{qrnt} = \{0, 0.1, \ldots 0.9, 1\}$.

With this study we aim towards a qualitative, general-purpose oriented model, rather than a model tuned to a specific dataset, region, or time frame, such that we use averaged fixed infectious parameters in our experiments, similar to other ABM approaches [30–33]. However, to prove that our model can fit real data, we present several fitting results in the Supplementary Materials Sections S1 and S2. Here, we use daily infectious and deaths data on COVID-19 from Romania and Hungary during October 2020–June 2021.

In contrast to our complex system approach on modeling and analyzing epidemic spreading, complementary studies employing an analytic approach in epidemics [5,34,35] include a time-dependent transmission rate to model changes in the infection rate caused by viral strain evolution, seasonality, social interactions, or governmental policies. Complementary to the differential equations of the compartmental models applied on the recent COVID-19 pandemic [5,34,35], ABMs study models of global mobility mechanisms based on emergent transmission dynamics. In this study, instead of a variable transmission rate, we use distributed simulation on the ABM resulting in a complex emergent population mixing instead of the compartmental models based on random uniform contact networks that are typically used to study epidemics spreading. Thus, modeling and quantifying human mobility is critical for studying large-scale spatial transmission of infectious diseases [31,32,36].

We note that the epidemic model considered in this study does not take into account active virus mutations, which means that it cannot simulate multiple outbreaks that arise from new strains. Instead, the model focuses on examining the dynamics related to quarantine for a single virus strain, i.e., the original SARS-CoV-2 strain. Nevertheless, in order to adjust the SICARQD model to another virus or strain, it suffices to redefine the seven parameters in Table 1 according to the available epidemiological data.

**Table 1.** Parameter setting for the SICARQD epidemic model, highlighting the values found in the literature, the values chosen in our model, and the supporting references. [1] Assumed worst case scenario based on literature review. [2] Parameters are being investigated in our study.

| Parameter Name | Model Parameter | Value in Literature | Value in Model | References |
|---|---|---|---|---|
| Infection rate | $\lambda_{inf}$ | 0-5% | 5% [1] | [24,37] |
| Incubation period | $\lambda_{ctg}$ | 5–7 days | 5 days | [38,39] |
| Delay—contagion to onset | $\lambda_{awr}$ | 4–7 days | 5 days | [37,38] |
| Delay—onset to recovery | $\lambda_{rec}$ | 10–14. . . 56 days | 14 days | [40–42] |
| Death ratio | $r_{death}$ | 1–3.4% | 3.4% [1] | [41,43] |
| Recurrence rate | $\lambda_{rcr}$ | 3–12 months | $3/12/\infty$ months [2] | [26,29] |
| Quarantine ratio | $r_{qrnt}$ | – | 0–100% [2] | |

### *2.3. The Spatial Agent-Based Model*

We start from the premise that social agents will move freely within a delimited area, such as a human settlement, or more specifically, an airport, a shopping mall, a hotel, a university campus, a conference venue, etc. In this sense, we define a two-dimensional rectangular space $S = 1600 \times 1200$ inside which we define a number of $N$ agents to serve as the simulation population. All agents are considered equal and uniformly distributed inside the space $S$. By keeping the area size fixed, we influence the population density $\rho = N/S$ through the population parameter $N$.

Next, we assign each agent $a_i$ a $home_i$ location, given by randomly generated coordinates $(hx_i, hy_i)$, and a point of interest (POI) $poi_i$ location given by a second set of coordinates $(px_i, py_i)$, generated based on the home location. More precisely, the POI is assigned by generating a power-law distributed distance $d_i$ from the home location,

then a random angle is chosen to define the direction of the POI location. The distance is calculated as follows:

$$d_i = d_{max} * ((\phi_m - 1) * d_{min} * rand(0,1))^{-1*\phi_m}$$
$$d_i = max\{min\{d_i, d_{max}\}, d_{min}\} \quad (1)$$

Two constants are defined in Equation (1), namely a minimum distance to the POI of $d_{min} = 100$ and a maximum distance to the POI of $d_{max} = 1000$. Both values are based on the chosen space $S$ and on empirical analysis through simulation. The two constants are also used to limit all values of generated distances within $[d_{min}, d_{max}]$. Another important parameter of the model, introduced in Equation (1), is the mobility factor $\phi_m$. This factor determines how close (contracted) or far away (expanded) the population is when referring to its mobility patterns. A smaller $\phi_m$ will generate more distant POIs and vice versa. Based on the parameters of the model mentioned above, we found the interval $1.05 \leq \phi_m \leq 1.5$ that allows us to simulate restriction policies in the agent-based model. For a chosen mobility factor or $\phi_m = 1.1$ we obtain a distribution of POI distances with a power-law exponent of $-2.3$ (measured using the *poweRlaw* package in R). Power-laws are found in many empirical studies to represent the realistic distribution of human activity, interactions, and mobility [44,45].

Each agent $a_i$ continuously moves between its home and POI (e.g., school, workplace, mall, grocery store, restaurant); its position at any time is given by the coordinates $(x_i, y_i)$. The movement towards a POI (and back home) is implemented by adjusting the current coordinates with a constant node speed on the horizontal and vertical axes, resulting in a 45-degree movement in one of four possible directions: NW, NE, SE, SW. Once the same coordinate as the POI is reached on either axis, the agent will move straight until the POI is reached. This intuitive process is explained in Figure 2a.

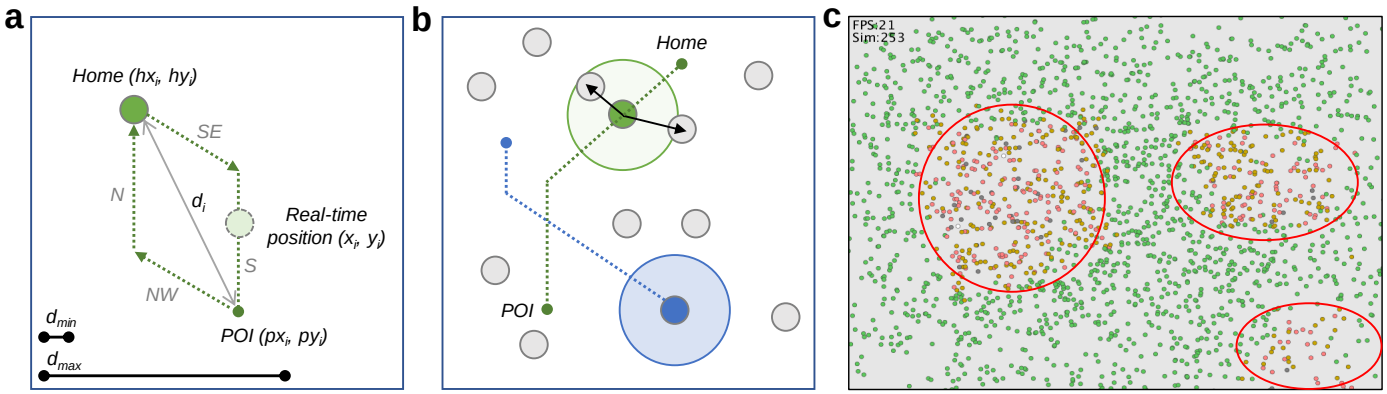


**Figure 2.** Overview of the agent-based model. (**a**) The relationship between an agent's home, POI and real-time locations. An agent will move to a POI (and back home) based on a combination of 45-degree directions followed by orthogonal movement. In the lower-left corner, the minimum and maximum POI distances are illustrated relative to the exemplified simulation space. (**b**) Multiple agents in the simulation space, of which two are highlighted with green and blue. Each agent moves independently to its POI and back. Each infected agent has an infection radius around which it can infect other susceptible agents based on the infection rate. (**c**) A screenshot from the simulation tool developed in Processing for educational purpose. Here, three initial infection clusters (orange and red dots) emerge and spread out based on each agent's mobility to engulf a larger population.

As the same mobility process is repeated for each agent $a_i$, a stochastic mixing of the population emerges. Here comes into play the SICARQD epidemic model. That is, almost every agent is initialized as susceptible $S$, except for several seed agents $N_s$ that are initially infected. In our experiments, we set the total population to $N \in \{1000, 2500, 5000\}$ agents and the number of seed agents $N_s = 25$ (0.5–2.5% of the population).

An infectious agent $a_i$ (i.e., contagious or aware, but not quarantined) will infect any other agent $a_j$ found in its real-time vicinity based on the infection rate $\lambda_{inf}$. The infection distance is set to 4× the agent size = $4 \times 8 = 24$ [30,46]. This process is exemplified in Figure 2b. Since we run a discrete event simulation, we define the discrete simulation time $t$, where $0 \leq t \leq K$, $K$ being the maximum simulation length. More precisely, we impose two stop conditions for our experiments: either a number of $K = 5000$ iterations are completed, or the number of infected agents drops to two or less, i.e., $I(t) + C(t) + A(t) + Q(t) \leq 2$. We chose these values on the basis of running several calibration experiments.

Based on the terms introduced, we quantify the effects of the epidemic using the following parameters: the epidemic size over time $0 < \phi(t) \leq 1$ (expressed as the ratio of the total infected population), the peak infected ratio $0 < \psi \leq 1$ (expressed as the maximum ratio of the infected population throughout the simulation), and the residual infection ratio at the end of the simulation $0 \leq \theta < 1$. The epidemic size, or the ratio of the total infected population $\phi(t)$ at any time $t$, is measured as follows:

$$\phi(t) = \frac{1}{N}[I(t) + C(t) + A(t) + Q(t)] \tag{2}$$

The peak infected ratio $\psi$, measured at the end of the simulation time $t = K$, is expressed as follows:

$$\psi = max\{\phi(t)\}, \ for \ 0 \leq t \leq K \tag{3}$$

The residual infection ratio $\theta$, measured as the average epidemic size over the last 50 iterations, is expressed as follows:

$$\theta = \frac{1}{50} \sum_{t=K-50}^{K} (\phi(t)) \tag{4}$$

To further explain the way our simulation environment is initialized, how the agents' position and infectious status are updated, and what the simulation framework measures, we provide Algorithm 1 with the goal of clarifying the relationship between the ABM and the epidemic model.

The spatial agent-based model presented and the embedded SICARQD epidemic model are implemented both as a Java applet with a user interface (UI) in the language *Processing* (mainly for educational purposes at our university; exemplified in Figure 2c), as well as in classic *Java* language for running the large-scale simulations (from the console) presented in the next section.

**Algorithm 1** Infectious status and position updates for any agent $a_i$ during each iteration $t$

**procedure** SETUPABM($A, S = [w \times h]$) ▷ Agent and POI placement
  **for** $\forall a_i \in A$ **do**
    $home_i(hx_i, hy_i) \leftarrow random([0, w], [0, h])$ ▷ Random within $S = [w \times h]$
    $d_i \leftarrow d_{max} \cdot ((\Phi_m - 1) \cdot d_{min} \cdot random(0, 1))^{-\Phi_m}$
    $\alpha_i = random(2\pi)$
    $poi_i(px_i, py_i) \leftarrow (d_i \cdot sin(\alpha_i), d_i \cdot cos(\alpha_i))$ ▷ Must be inside $S$, else regenerate
  **end for**
**end procedure**
**procedure** UPDATEAGENTS($A, SICARQD, t$) ▷ Agent update
  **for** $\forall a_i \in A$ **do**
    **if** $a_i.state = D$ **then** continue; ▷ Ignore dead agents
    **end if**
    update $a_i.status(t+1) \leftarrow (a_i.status(t), SICARQD)$ ▷ Update infection status
    update $a_i(x_i, y_i) \leftarrow (d_x, d_y)$ ▷ Update position towards home or POI
  **end for**
  **for** $\forall (a_i, a_j) \in A$ **do**
    **if** distance$\{a_i, a_j\} \leq$ infection distance **then** ▷ Check agent–agent interaction
      **if** $a_i.state = I$ & $a_j.state = S$, with $\lambda_{inf}$ **then**
        $a_j.state \leftarrow I$
      **end if**
      **if** $a_j.state = I$ $l$; & $a_i.state = S$, with $\lambda_{inf}$ **then**
        $a_i.state \leftarrow I$
      **end if**
    **end if**
    update(S,I,C,A,R,Q,D)
  **end for**
  $\phi(t) \leftarrow 1/N \cdot (I + C + A + Q)$
**end procedure**

## 3. Results

The experimental setup consists of repeated discrete event computer simulations that alter one of the following model parameters: quarantine policy, patient recurrence rate, ratio of quarantined infected population, and agent population size. Specifically, the three quarantine policies are proactive, reactive, and no quarantine (see Section 2.1); the three epidemic recurrence scenarios are short, long, and never recur (see Section 2.1); the quarantine ratios range within $r_{qrnt} \in \{0, 0.1, \ldots 0.9, 1\}$; population size ranges within $N \in \{1000, 2500, 5000\}$. Furthermore, the duration of the simulation is limited to $K = 5000$ iterations or until the number of infected agents drops back to two (or fewer) agents. We made several considerations to simplify the analysis of all simulation results, such as: (i) treating all social agents as identical, (ii) limiting the agent population to reduce simulation time, (iii) assigned a reasonable amount of infectious spreader agents (i.e., $|N_s| = 25$, which corresponds to ≈2% of all agents in the network), (iv) assigned power-law distributed travel distances to all agents in the same manner, (vi) fixed a long enough simulation duration to allow convergence of the epidemic size in time.

To ensure statistical validity, all experimental results represent the average values measured over 100 repeated simulations using the same settings. Overall, we conducted a total of 3 (quarantine policies) ×3 (recurrence scenarios) ×11 (quarantine ratios $r_{qrnt}$) ×3 (population sizes $N$) ×100 (repetitions) = 29,700 experiments that correspond to 297 unique simulation settings. Therefore, we prefer to provide a graphical representation of the numerical results in various settings rather than providing unusually long tables. To fully recognize the impact of each simulation parameter, we study the results using the graphical representations in Figures 3–8.

We first measure the infected population ratio $\phi(t)$ (i.e., total number of infected relative to the whole population, at every moment in time) by comparing the proactive

(proact-Q) and reactive (react-Q) quarantine policies for the never-recurrence scenario (never-R). Figure 3 details the two quarantine policies for three representative quarantine ratios ($r_{qrnt} = \{0.2, 0.6, 0.8\}$). By adopting a proactive quarantine, as illustrated in Figure 3a, a distinctive impact of the quarantine ratios becomes visible. The measured peak infection ratios are $\psi = 0.36$ (for $r_{qrnt} = 0.2$ quarantined infected patients), respectively, $\psi = 0.14$ (for $r_{qrnt} = 0.6$ quarantined) and $\psi = 0.036$ (for $r_{qrnt} = 0.8$ quarantined). The differences measured in $\psi$ result in a decrease of approximately 61% in the size of the epidemic when the strength of the quarantine increases from 20% to 60%, and another 74% when the quarantine is strengthened further to 80%. A noticeable effect of increasing the quarantine ratio past 0.6 is that the duration of the epidemic increases significantly. On the other hand, by adopting the reactive quarantine depicted in Figure 3b the impact of the quarantine ratio is significantly reduced. We measure a drop of 17% from $\psi = 0.41$ (for $r_{qrnt} = 0.2$) to $\psi = 0.33$–$0.34$ (for $r_{qrnt} = 0.6$–$0.8$). Additionally, comparing the numerical results in Figure 3a,b, we notice an increase in the epidemic size determined by switching from proact-Q to react-Q. The increases are 14% for $r_{qrnt} = 0.2$, 43% for $r_{qrnt} = 0.6$, and more than 700% for $r_{qrnt} = 0.8$.

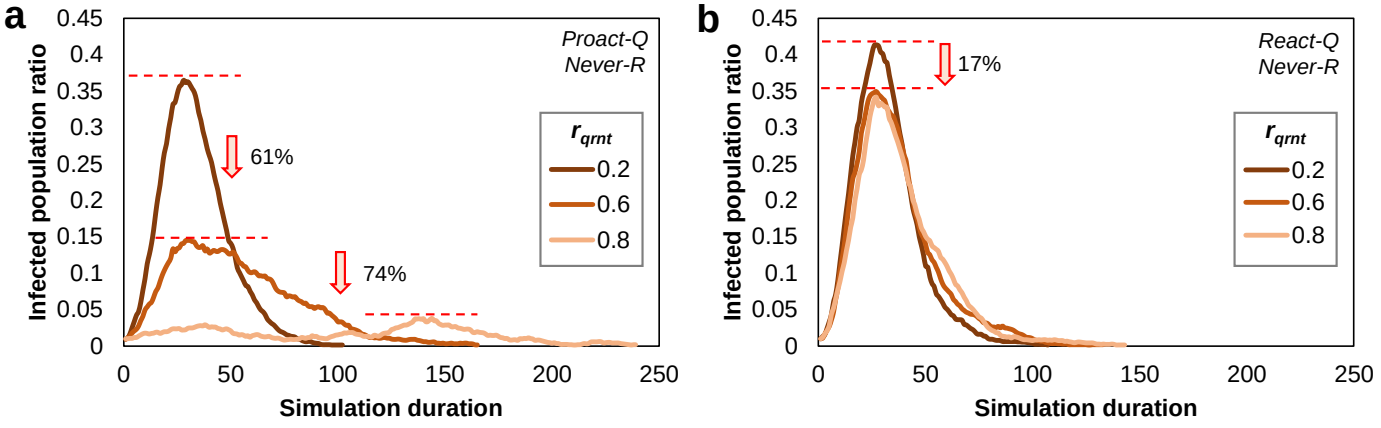


**Figure 3.** Overview of the evolution of an epidemic outbreak without patient recurrence (never-R), in time, measured by the infected population ratio $\phi(t)$. (**a**) The proactive quarantine policy (proact-Q) is applied. (**b**) The reactive quarantine policy (react-Q) is applied. The relative drops in infected population are depicted in percentages.

Next, in Figure 4 we aim to highlight the impact of quarantine policy on the total infected population ratio and the peak infection ratio. Given a long-recurrence (long-R) scenario, we notice very distinctive evolution patterns of the epidemic outbreaks. In Figure 4a, in terms of the total population infected throughout the simulation, when no agents are quarantined (i.e, $r_{qrnt} = 0$, up to 120% of the population becomes infected; this value results from counting all new infections that occur before the outbreaks dampen. In case of no-Q, the $r_{qrnt}$ parameter does not have an influence, therefore, the infected population remains at 120%. In the case of react-Q, we measure a slight drop of 21% with increasing quarantine ratio. Finally, in the case of proact-Q, we observe an almost complete reduction (>99%) of the epidemic. However, more important is the visible phase transition around the values $r_{qrnt} = 0.6 - 0.8$, when for just a 20% strengthening of quarantine, a 92% relative drop of the total infected population is triggered. In Figure 4b, the decrease in the peak infected ratio $\psi$ is similar to the total infected ratio, for the no-Q and react-Q policies; we measure an average drop of 28% for $\psi$ for react-Q. The evolution of the peak infected ratio for proact-Q is different from the total infected ratio in the left panel; here, we see an almost perfectly linear drop with the quarantine ratio. The amplitude of the highest epidemic wave is 47% given the simulation parameters described.

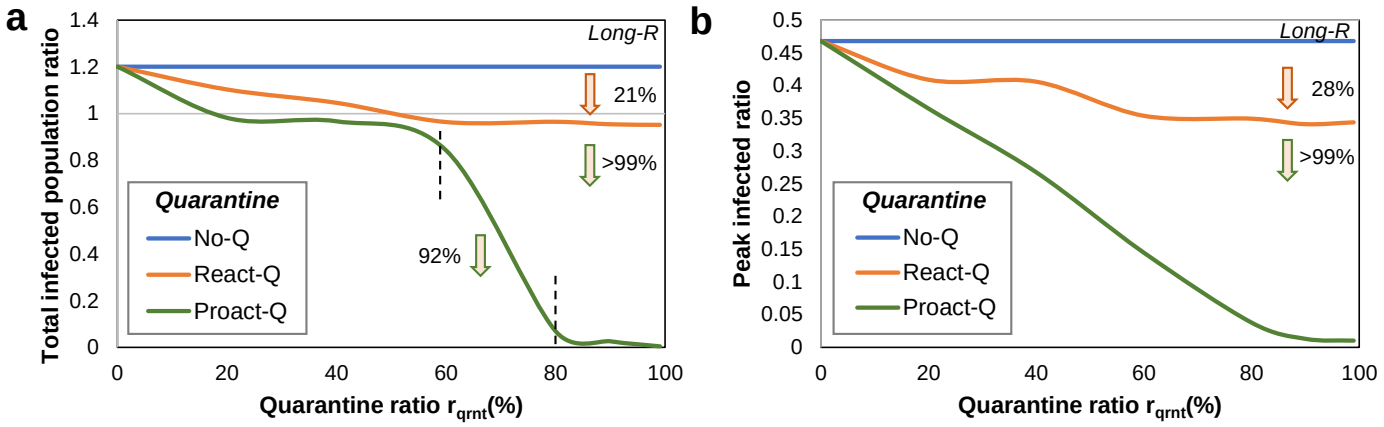


**Figure 4.** Impact of each quarantine policy in terms of an increasing quarantine ratio $r_{qrnt}$. (**a**) The total infected population ratio measured as the sum of all new cases throughout the simulation until the epidemic dissipates. The two vertical dotted bars delimit the phase transition area between $r_{qrnt}$ = 0.6–0.8. (**b**) The peak infection ratio expressed as the maximum amplitude of the epidemic wave relative to the population of agents. The percentages along the right border of each panel represent relative decreases from the maximum to the minimum infected ratio.

Next, in Figure 5 we emphasize the impact of the patient recurrence rate on the total infected population. In Figure 5a we apply a reactive quarantine policy and notice a significant difference in epidemic size between short-R, on the one hand, and long-R and never-R, on the other. In the case of a rapidly recurring disease (i.e., short-R) as many as $\times 3$ of the total population becomes infected throughout the epidemic; practically, each agent is infected, on average 3 times. However, if the immunity granted is about one year or more, the total infected ratio drops to 1–1.2 $\times N$, which means that all agents will become infected approximately once. The drops in the total infected ratio are small, of about 19–21% as the quarantine ratio increases. In case of a proactive quarantine policy, as depicted in Figure 5b, the epidemic impact is significantly reduced with increasing $r_{qrnt}$. Specifically, the same phase transition mentioned previously occurs between $r_{qrnt}$ = 0.6–0.8, where we register drops in the total infected ratio of 85% for the short-R scenario, 60% for the long-R scenario, respectively, 92% for never-R.

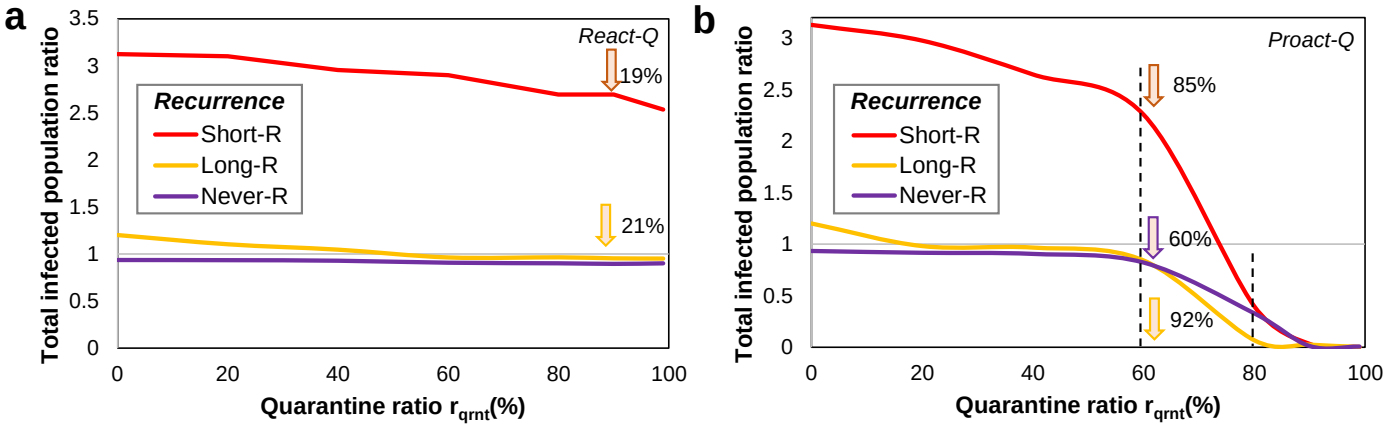


**Figure 5.** Impact of the recurrence scenario in terms of an increasing quarantine ratio $r_{qrnt}$. (**a**) The total infected population ratio measured for a reactive quarantine policy. (**b**) The total infected population ratio measured for a proactive quarantine policy. The two vertical dotted bars delimit the phase transition area between $r_{qrnt}$ = 0.6–0.8; the respective decreases in the infected population ratios are displayed in relative percentage for each scenario of recurrence.

Our next analysis focuses on the dynamics of the infected population ratio $\phi(t)$ from the perspective of two fixed quarantine ratios. In Figure 6 we chose to depict the two ratios that delimit the phase transition previously observed, namely $r_{qrnt} = 0.6$ and $r_{qrnt} = 0.8$. We keep the recurrence scenario fixed to long-R and observe the qualitative differences between the three quarantine policies. Figure 6a corresponds to the snapshot of the epidemic before the phase transition triggers, and we easily distinguish between quarantine policies. The highest peak infection ratio is determined by a no-Q policy; the react-Q policy reduces the maximum infection ratio by 23%, and the proact-Q policy further reduces the infection ratio by 59%. Figure 6b corresponds to the measurements after the phase transition has been initiated, and, again, we can easily distinguish between quarantine policies. The highest peak infection ratio is determined by the no-Q policy, followed by the react-Q policy, which reduces the infection ratio by 26%. The proact-Q policy further reduces the infection ratio by up to 89% compared to react-Q. Although the duration of the proact-Q epidemic increases, the total infected ratio remains much smaller than for the other two quarantine policies. When comparing the green line infected ratios $\phi(t)$ for proact-Q, in the two panels, we measure a relative decrease of 74%.

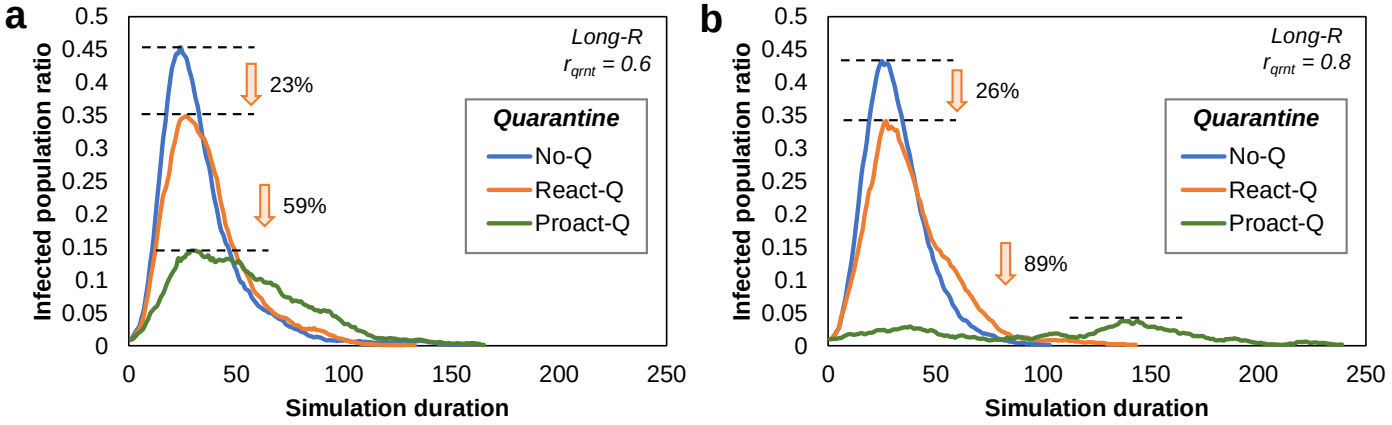


**Figure 6.** Overview of the evolution of epidemic outbreaks with long patient recurrence (long-R) from the perspective of the three quarantine policies. (**a**) The quarantine ratio is set to $r_{qrnt} = 0.6$, before which the phase transition in the infected population ratio occurs. (**b**) The quarantine ratio is set to $r_{qrnt} = 0.8$, after which the phase transition in the infected population ratio occurs. The decreases in the infected population ratios are shown as relative percentage for each quarantine policy.

In addition to the previous analysis, in Figure 7 we further illustrate the significant effect of the restrictiveness of quarantine, measured by the three quarantine ratios $r_{qrnt} = 0.2$, $0.6, 0.8$. In all simulations, we use the proactive quarantine policy (proact-Q). Figure 7a exemplifies the evolution of the infected population ratio $\phi(t)$, in what we call a "less restrictive" quarantine, given by the small $r_{qrnt} = 0.2$. Although the long-R and never-R scenarios are characterized by a single epidemic wave, the short-R scenario leaves a significant residual (ongoing) infection of $\theta \approx 12\%$ in the population, with subsequent smaller waves. The peak infection rate for all recurrence scenarios is $\psi = 0.36$, but only short-R remains active throughout the duration of the simulation. In Figure 7b we observe a drop in the peaks of all epidemics. Notably, for this "moderately restrictive" quarantine ($r_{qrnt} = 0.6$), the peak of the short-R scenario drops to $\psi = 0.2$, by 44% compared to the "less restrictive" quarantine. The other two recurrence scenarios reduce the peaks even further to $\psi$ = 0.13–0.14, and their corresponding epidemics dissipate. Again, the short-R scenario leaves a significant residual infection of $\theta \approx 10\%$ in the population, with subsequent smaller waves. Figure 7c presents the infected population ratio by adopting a "highly restrictive" quarantine, given by the higher $r_{qrnt} = 0.8$. Here, all recurrence scenarios are greatly dampened, and we measure infection peaks of only $\psi$ = 0.002–0.038. Thus, the short-R peak is reduced by 81% compared to the peak measured for $r_{qrnt} = 0.6$;

nevertheless, larger secondary epidemic waves are produced (around $t$ = 150–200) even in case of the highly restrictive quarantine. In this case, only a negligible amount of residual infection of $\theta \leq 1\%$ remains in the population at the end of the simulation.

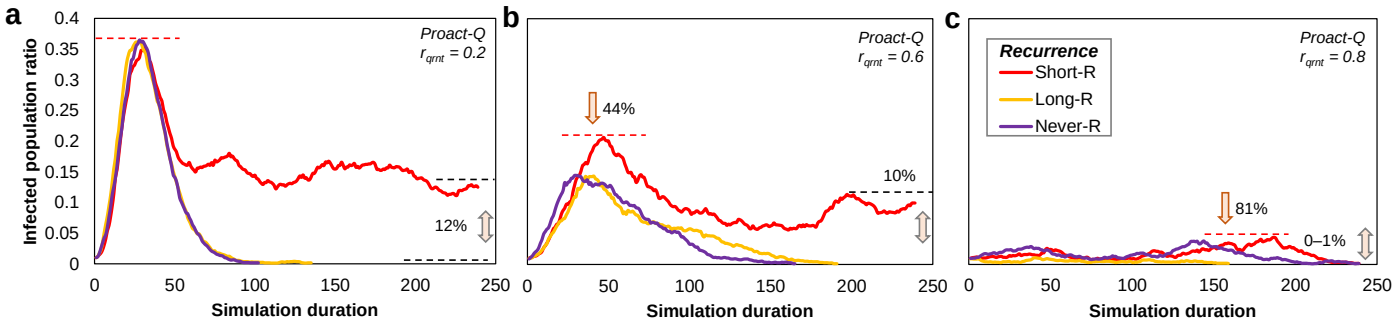


**Figure 7.** Evolution of epidemic outbreaks in time by employing a proactive quarantine policy (proact-Q) from the perspective of the three recurrence scenarios, using different quarantine ratios in each of the three panels. (**a**) A "less restrictive" quarantine ($r_{qrnt} = 0.2$) which triggers the highest infection peaks ($\psi = 0.36$) for all recurrence scenarios. The short-R scenario leaves a residual (ongoing) infection of 12% at the end of the simulation. (**b**) A "moderately restrictive" quarantine ($r_{qrnt} = 0.6$) which lowers the infection peaks ($\psi = 0.20$ for short-R, in red) for all recurrence scenarios. Again, the short-R scenario leaves a residual infection of around 10%. (**c**) A "highly restrictive" quarantine ($r_{qrnt} = 0.8$) which lowers the infection peaks even further ($\psi$ = 0.002–0.038) for all recurrence scenarios. Almost no residual infection remains in the population. The decreases in the peak infection ratio for short-R (red) are displayed for the quarantine ratios $r_{qrnt} = 0.6, 0.8$ relative to the highest peak measured for $r_{qrnt} = 0.2$.

Finally, we discuss the impact of population density in the agent-based model. Figure 8 shows the infected population ratio $\phi(t)$ in two different scenarios that we consider representative of the entire experimental setup. In Figure 8a we apply a reactive quarantine and a short recurrence to distinguish between the evolution of three different populations. The largest agent population, $N = 5000$, results in the highest population density, which is translated into the most impactful outbreak. To this end, we measure a peak of $\psi = 0.68$ followed by a permanent infected ratio of $\phi(t) \approx 25\%$ (caused by the short-R scenario). The smallest population of $N = 1000$ produces a peak of only $\psi = 0.28$ and a lower residual infection rate of $\theta \approx 10\%$. The reduction in the peak infection rate is 38% if the population is reduced to $N = 2500$, and further by 33% for $N = 1000$. By contrast, in Figure 8b we employ a proactive quarantine and a long recurrence to distinguish between the evolution of three different populations. The largest population produces a peak of $\psi = 0.36$ followed by a permanent infected ratio of $\phi(t) \approx 5\%$. The smallest population produces a peak of $\psi = 0.083$ and a lower residual infection rate of $\theta \leq 1\%$. The peak infection rate decreases by 31% if the population is reduced from $N = 5000$ to $N = 2500$, and further decreases by 67% for $N = 1000$.

An important remark is that we did not plot the 95% confidence intervals (SD or any similar statistical reliability measure) for any of the plots in the results section because it would add a lot of complexity to the already detailed plots. However, all results from each experimental set-up present reliable convergence over the 100 repeated simulations. In our numerical analysis, we found that the maximum deviation from the plotted averages is not greater than $\pm 3\%$.

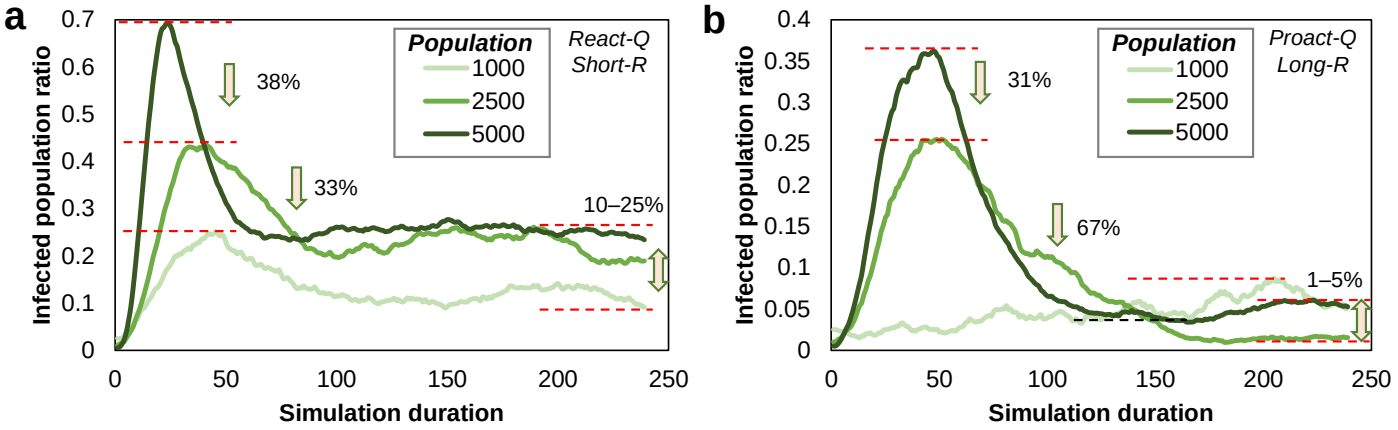


**Figure 8.** The impact of the population density on the evolution of epidemic outbreaks measured by $\phi(t)$. Note that density is proportional to the population size $N$, as we keep the simulation space $S$ fixed. (**a**) A reactive quarantine policy and a short recurrence determine high infection ratios in the population (up to $\psi = 0.68$). A final, residual infection rate of 10–25% remains until the end of the simulation time. (**b**) A proactive quarantine policy and a long recurrence determine relatively lower infection ratios (up to $\psi = 0.36$). A final, residual infection rate of 1–5% remains until the end of the simulation time. The decreases in the peak infected ratio are shown as relative percentage for each population size $N$.

## 4. Discussion

Agent-based modeling is an effective interdisciplinary means of tracking and controlling epidemics, capable of incorporating the stochasticity of human behavior, which remains unaccounted for with just the classical compartmental model approach [4,5,47,48]. Specifically, by combining a spatial ABM with our proposed SICARQD epidemic model, we can replicate, monitor, and understand the parameters that affect the control of large-scale epidemics, with an overarching impact in epidemiology, mathematical modeling and public health, which are all very important social and scientific challenges [1,2,49,50].

In this study, we devise a spatial ABM represented by a closed-space agent population, in which agents receive two generated locations—a home and a point of interest—between which they continuously travel back and forth. The emergent mobility patterns result in a stochastic mixing of agents that replicates the real-world transmission of airborne diseases between each other (i.e., through physical proximity) to distances greater than their own vicinity. Furthermore, we take our previously introduced COVID-19 specific SICARS epidemic model [11] and augment it to a more elaborate model that: (i) can be used to incorporate quarantine policies (e.g., time and strength of these) and different patient recurrence rates, (ii) and can be parameterized to different viruses based on available epidemiological data.

We are able to reproduce similar epidemic dynamics to that of time-dependent transmission rates [34,35] to account for the social interaction and variable policies, by modeling and controlling the spatio-temporal movement of contagious and healthy agents through discrete event computer simulation [31,32]. Therefore, we defined a stochastic mobility model for agents and integrated an epidemic model to account for the specific SARS-CoV-2 transmission rates to provide a qualitative overview that emphasizes global perception of the complex system.

Compared to the classic infected ($I$) state of the SIR model, in SICARQD we define three different infected states: incubating $I$ (timeout period from contracting a virus until the patient becomes a spreader), contagious $C$ (first state in which the patient infects its peers, but without displaying symptoms), and aware $A$ (second state in which the patient infects peers, but with symptoms). The details of our SICARQD model are illustrated in Figure 1. Furthermore, we address the issue of quarantine, which represents another possible patient state ($Q$). By controlling when and how many patients transit to $Q$, we

can simulate different levels of policy and restriction (using the $r_{qrnt}$ parameter). To this end, we analyze a proactive quarantine policy (proact-Q) that is applied before the patient becomes contagious, a reactive policy (react-Q) that is applied before the patient becomes aware, and no quarantine at all (no-Q). In a public health system, these policies can be applied by continuous contact tracing (proact-Q) or by intensive testing (react-Q). Another parameter we aim to study is the impact of the disease recurrence rate; in this sense, we consider a short recurrence (short-R) of 3 months, a long recurrence (long-R) of 1 year, and no recurrence (never-R). The purpose of adding these parameters to SICARQD is to observe whether (i) proactive quarantine is worth the extra costs, (ii) whether more restrictive quarantine has an impact on reducing the outbreak size, and (iii) whether the patient recurrence rate plays an important role in our efforts to mitigate the disease spreading.

We rely on discrete event simulation using a custom-developed computer program (using Processing and Java) to implement the described methodology. A total of 297 unique simulation scenarios were run, each repeated 100 times, and their results were averaged. Our results focus on the qualitative aspects of the described epidemiological policy parameters rather than replicating a specific geographical setting or demographic constraints.

The main observations drawn from our experiments are explained in the following three paragraphs. The proactive quarantine policy in correlation to a higher quarantine ratio (i.e., stricter quarantine policy) triggers a phase transition that reduces the total infected population by more than 90%, compared to reactive quarantine. Therefore, a proactive quarantine policy associated with a strict quarantine ratio can almost entirely inhibit infectious spreading, compared to a reactive quarantine which limits infectious spreading by about 20%, compared to no quarantine at all.

Indeed, proactive quarantine policy plays a significant role in reducing the peak infection rate, but only if combined with a more restrictive isolation of $>$60% quarantined infected patients. Specifically, when restrictiveness increases from 20% to 60%, the epidemic size decreases by 61% (see Figure 3). By increasing the restrictiveness to 80%, we can drastically reduce the peak infection ratio by another 74% relative to the previous peak. In contrast, if we rely on reactive quarantine, then the impact of increasing quarantine restrictiveness is relatively small, a reduction of just 17% on the infection peak. Furthermore, we investigated the restrictiveness interval 60-80% where we found a phase transition in the epidemic size; namely, the reduction of the epidemic is significant, by up to 92% if we increase the restrictiveness by only 20%. Of course, in real-world settings it is difficult to achieve an 80% isolation of infected patients, but the rewards of achieving such an isolation level are very high (see Figure 4).

The recurrence rate plays a very important role in terms of the total infected population over the course of the epidemic. Although the amplitude of epidemic waves for short-R remains similar to that of long-R, a residual (ongoing) infection remains in the population, with subsequent smaller waves, which add up to the total number of infected. More precisely, approximately $\times$3 times more agents are infected compared to long-R and never-R. However, all recurrence scenarios are positively influenced by the increase in quarantine restrictiveness, since we measure similar phase transitions in epidemic size, with drops of 85%, 60% and 92% for the short-R, long-R, and never-R recurrence scenarios (see Figure 5). Furthermore, as supported by our analysis of the population size (see Figure 8 for details), we found that the short recurrence scenario (short-R) significantly favors the epidemic to remain active on the long-term. Here, we suggest that short-R may determine a residual infection ratio of 10–25% in the population. When switching to a long-R scenario, the residual infection ratio remains within a more manageable 1–5% of the population.

The timing of quarantine is an important parameter that directly influences the peak infection ratio (i.e., amplitude of the highest wave). For a moderately restrictive quarantine ($r_{qrnt} = 0.6$), a no quarantine policy (no-Q) translates into having a peak infection ratio of 44% of the population, versus 34% if a reactive quarantine policy is adopted; furthermore, the peak can be reduced to 14% if a proactive policy is enabled. For a highly restrictive

quarantine ($r_{qrnt} = 0.8$), no-Q induces a similar peak of 43%, versus a similar 32% peak if react-Q is adopted, and a much smaller peak of 3.4% if proact-Q is adopted (see Figure 6).

The emergence of a residual infection and subsequent larger outbreaks is an ongoing and important debate in the recent literature on COVID-19 [51,52]. Within our simulation framework, we can reproduce this residual infection rate, as well as impactful secondary epidemic waves, based on the adopted recurrence scenario. Specifically, if we simulate a short recurrence, in which patients can reinfect, on average, in less than 6 months [26,27], we obtain approximately 1–12% remaining infected individuals after the first wave. This percentage decreases with an increase in the quarantine ratio, but even for highly restrictive quarantine, like $r_{qrnt} = 0.8$, we notice a larger secondary wave in Figure 7c. The epidemic recurrence phenomenon is induced by the emergent agent mobility modeled in our system. More precisely, recovered agents lose their immunity in time and travel to infected areas before the hotspots dissolve, and so, hotspots may be maintained for very long durations (e.g., several years). The suggested solution against these residual hotspots—based on our ABM results—is mobility reduction and proactive quarantine policies.

The general observations validated throughout the experiments are summarized as the following guidelines:

- The peak infected ratio (i.e., amplitude of the highest epidemic wave) is reduced in the following scenarios:
    1. By increasing the quarantine restrictiveness in our model through the $r_{qrnt}$ parameter. Specifically, a phase transition is observed in the infected ratio when isolating more than 60% of the infected population. More precisely, the decreases in infection ratio, when increasing $r_{qrnt} = 0.6$ to $r_{qrnt} = 0.8$, range between 60-92% (when proactive quarantine is applied, see below).
    2. By combining the restrictiveness with a proactive quarantine policy, rather than a reactive one. This means isolating suspicious cases early, before they become contagious through population-wide contract tracing and testing. The proactive quarantine policy will reduce the peak infection ratio by 59–89% compared to the reactive policy.
    3. In less densely populated areas. This may be achieved again by partial isolation or relocation of the population.
- The total infected population (i.e., total number of new cases throughout the simulation) is reduced in the following scenarios:
    1. If the patient recurrence rate is longer: of one year, or more. In the short-R scenario (3 months), more than $\times 3$ people become infected compared to long-R (one year). A long recurrence rate can be achieved through natural immunity or through vaccination, depending on the virus.
    2. By applying the previously described solutions: a proactive quarantine policy combined with a greater restrictiveness of more than 60% isolation.
    3. In less densely populated areas. This may be achieved again by partial isolation or relocation of the population.
- The residual infection ratio (i.e., the infected ratio that remains in the population for a very long time) is reduced in the following scenarios:
    1. Depends primarily on the recurrence rate; a short-R scenario can leave a 10–12% infected ratio in the population, while the long-R and never-R scenarios help to completely dissipate the epidemic in time.
    2. Depends on the population density combined with the quarantine policy. A react-Q policy and a high population density can lead to a residual infection ratio of 10–25%, while a proact-Q can keep the residual infection ratio within 1–5%.

In essence, the proactive quarantine in correlation to a higher quarantine ratio (i.e., stricter quarantine policy) triggers a phase transition reducing the total infected population by over 90%, compared to the reactive quarantine. Therefore, a proactive quarantine associated with a strict quarantine ratio can almost completely inhibit infectious spread, compared

to a reactive quarantine which limits infectious spreading by about 20%, compared to no quarantine at all.

Some of the limitations of this study are discussed in more detail. First, our model is not able to fully capture the complexity of human behavior and interactions. However, while some ABM approaches focus on incorporating social aspects, such as agent age group [53], social similarity [36], or leisure activities [54], other models focus strictly on the complexity of human topology [32,33], mobility patterns [31] or computation [55]. In this sense, our model offers a contribution in regard to mobility patterns based on POIs, which have been proven to represent infection hotspots in dense areas [20]. Second, the closed space in which the agent population is allowed to move restricts the study of a very large-scale, heterogeneous, or hierarchical population model. However, a hierarchical ABM can be defined where each ABM corresponds to a neighborhood or a town in a larger geographic area, similar to the study in [56]. Third, the agents are considered identical; they travel with the same speed, each has one single point of interest (POI), and we did not add any demographic data like age groups or gender. However, our study focuses on the broader perspective of quarantine policies and recurrence rates, rather than on specific geo-social settings. Still, the ABM can be further developed to incorporate multiple POIs and some individual traits. Fourth, we tuned the SICARQD epidemic model with data specific to the SARS-CoV-2 virus. As such, the numerical estimations may change with other future viruses. A simple re-tuning of the model will suffice to adapt to new epidemic situations. Lastly, our SICARQD epidemic model does not consider asymptomatic cases. However, given the high number of unaccounted asymptomatic cases during the COVID-19 pandemic, the actual number of agents entering the aware state would be slightly reduced and the efficiency of the react-Q policy could drop (i.e., they cannot become aware without symptoms). This effect may stack up among recurrent infections.

In addition to the scientific potential of our proposed methodology, our results find immediate applicability in the real world in the context of COVID-19, as well as future pandemics with similar transmission mechanisms. Furthermore, the enumerated observations can be further adopted in social physics, by corroborating our epidemic control strategies with opinion injection strategies and competing influence dynamics [57–59], or other immunization strategies for viral outbreaks [60,61].

## 5. Conclusions

The design of effective strategies for the tracking and control of epidemics is a major concern for public health systems around the world and an ongoing scientific challenge [1–3]. Much of the current state-of-the-art work is either focused on *flattening the curve* solutions [4,5,14,62], or limited to specific geographic and demographic settings [16,17], or their epidemic models do not focus on various quarantine policies [18,19]. Therefore, our study integrates agent-based modeling with a novel epidemic model to provide a qualitative study on quarantine policies and recurrence rates in large populations. Overall, our research is innovative because it targets policy makers by providing a set of "epidemic control guidelines" based on our simulation results.

Specifically, in this article, we study the effect of control procedures, implemented through quarantine timing and strength of isolation, from the perspective of variable patient recurrence rates, to understand their impact on containing epidemics over closed populations. In our SICARQD epidemic model, we incorporate three infectious states ($I$, $C$, $A$) and a quarantine state ($Q$) which allow for implementing an early (proact-Q) quarantine policy and a late (react-Q) policy. Therefore, by specifying *when* and *how many* patients transit to $Q$, we simulate different levels of policy and restrictiveness in the population. Furthermore, we introduce three possible recurrence scenarios (short-R, long-R, never-R), which aim to demonstrate the effectiveness of the quarantine policies with respect to the natural response of patients to an infectious disease. Consequently, by corroborating all parameters into our ABM, we provide a discrete event simulation framework for current and future epidemic scenarios.

Regarding the remarkable amount of published literature on epidemic outbreaks during the COVID-19 period, we strongly believe that our study represents a promising direction of research aimed at better understanding the real-world impact of quarantine policies, their timing and strength, and the impact of the natural disease recurrence rate in patients, all by incorporating real epidemiological data. In general, we consider that our proposed ABM framework can trigger the creation of computational intelligence tools to further enhance strategies for the monitoring and control of large-scale public health systems in a safe and effective manner.

Future research directions may include (i) incorporating hierarchical agent-based models to replicate more realistic human populations, (ii) integrating a set of vaccination strategies on top of the existing policies, (iii) defining multiple categories of agent types and adding additional mobility patterns, (iv) and refining the SICARQD model with epidemic data characteristic to specific regions around the world.

**Supplementary Materials:** The following are available online at https://www.mdpi.com/article/10.3390/math11061336/s1, Figure S1: Time series data on daily COVID-19 cases in Romania, Figure S2: Fitting data on daily infectious cases, Figure S3: Fitting data on daily deaths, Table S1: Fitting accuracy of the epidemic model for COVID-19 data. Reference [63] is cited in Supplementary Materials.

**Funding:** This research received no external funding.

**Data Availability Statement:** All data used in this study is summarized in Table 1 and is represented by epidemiological data for the SARS-CoV-2 virus responsible for the COVID-19 pandemic. The parameters were used to tune the introduced SICARQD epidemic model for the experimental setup presented; these parameters were taken from cited resources as follows: infection rate [24,37], incubation period [38,39], delay between contagion and onset [37,38], delay between onset and recovery [40–42], death ratio [41,43], and recurrence rate [26,29].

**Conflicts of Interest:** The author declares no conflict of interest.

## References

1. Keeling, M. The implications of network structure for epidemic dynamics. *Theor. Popul. Biol.* **2005**, *67*, 1–8. [CrossRef] [PubMed]
2. Keeling, M.J.; Rohani, P. *Modeling Infectious Diseases in Humans and Animals*; Princeton University Press: Princeton, NJ, USA, 2008.
3. Salathé, M.; Jones, J.H. Dynamics and control of diseases in networks with community structure. *PLoS Comput. Biol.* **2010**, *6*, e1000736. [CrossRef] [PubMed]
4. Hellewell, J.; Abbott, S.; Gimma, A.; Bosse, N.I.; Jarvis, C.I.; Russell, T.W.; Munday, J.D.; Kucharski, A.J.; Edmunds, W.J.; Funk, S.; et al. Feasibility of controlling COVID-19 outbreaks by isolation of cases and contacts. *Lancet Glob. Health* **2020**, *8*, e488–e496. [CrossRef] [PubMed]
5. Kucharski, A.J.; Russell, T.W.; Diamond, C.; Liu, Y.; Edmunds, J.; Funk, S.; Eggo, R.M.; Sun, F.; Jit, M.; Munday, J.D.; et al. Early dynamics of transmission and control of COVID-19: A mathematical modelling study. *Lancet Infect. Dis.* **2020**, *20*, 553–558. [CrossRef]
6. Koo, J.; Cook, A.; Park, M. Interventions to mitigate early spread of COVID-19 in Singapore: A modelling study. *Lancet Infect Dis.* **2020**, *20*, 678–688. [CrossRef]
7. Galea, S.; Riddle, M.; Kaplan, G.A. Causal thinking and complex system approaches in epidemiology. *Int. J. Epidemiol.* **2010**, *39*, 97–106. [CrossRef]
8. Siegenfeld, A.F.; Bar-Yam, Y. An introduction to complex systems science and its applications. *Complexity* **2020**, *2020*, 6105872. [CrossRef]
9. Adam, D. Special report: The simulations driving the world's response to COVID-19. *Nature* **2020**, *580*, 316–319. [CrossRef]
10. Hinch, R.; Probert, W.J.; Nurtay, A.; Kendall, M.; Wymant, C.; Hall, M.; Lythgoe, K.; Bulas Cruz, A.; Zhao, L.; Stewart, A.; et al. OpenABM-Covid19—An agent-based model for non-pharmaceutical interventions against COVID-19 including contact tracing. *PLoS Comput. Biol.* **2021**, *17*, e1009146. [CrossRef]
11. Topirceanu, A.; Udrescu, M.; Marculescu, R. Centralized and decentralized isolation strategies and their impact on the COVID-19 pandemic dynamics. *arXiv* **2020**, arXiv:2004.04222.
12. Diaz, P.; Constantine, P.; Kalmbach, K.; Jones, E.; Pankavich, S. A modified SEIR model for the spread of Ebola in Western Africa and metrics for resource allocation. *Appl. Math. Comput.* **2018**, *324*, 141–155. [CrossRef]
13. Arenas, A.; Cota, W.; Gomez-Gardenes, J.; Gómez, S.; Granell, C.; Matamalas, J.T.; Soriano-Panos, D.; Steinegger, B. A mathematical model for the spatiotemporal epidemic spreading of COVID19. *MedRxiv* **2020** . [CrossRef]
14. Ferguson, N.M.; Cummings, D.A.; Fraser, C.; Cajka, J.C.; Cooley, P.C.; Burke, D.S. Strategies for mitigating an influenza pandemic. *Nature* **2006**, *442*, 448–452. [CrossRef] [PubMed]

15. Mistry, D.; Litvinova, M.; y Piontti, A.P.; Chinazzi, M.; Fumanelli, L.; Gomes, M.F.; Haque, S.A.; Liu, Q.H.; Mu, K.; Xiong, X.; et al. Inferring high-resolution human mixing patterns for disease modeling. *Nat. Commun.* **2021**, *12*, 1–12. [CrossRef] [PubMed]
16. Hoertel, N.; Blachier, M.; Blanco, C.; Olfson, M.; Massetti, M.; Rico, M.S.; Limosin, F.; Leleu, H. A stochastic agent-based model of the SARS-CoV-2 epidemic in France. *Nat. Med.* **2020**, *26*, 1417–1421. [CrossRef] [PubMed]
17. Datta, A.; Winkelstein, P.; Sen, S. An agent-based model of spread of a pandemic with validation using COVID-19 data from New York State. *Phys. A Stat. Mech. Appl.* **2022**, *585*, 126401. [CrossRef] [PubMed]
18. Frias-Martinez, E.; Williamson, G.; Frias-Martinez, V. An agent-based model of epidemic spread using human mobility and social network information. In Proceedings of the 2011 IEEE Third International Conference on Privacy, Security, Risk and Trust and 2011 IEEE Third International Conference on Social Computing, Boston, MA, USA, 9–11 October 2011, pp. 57–64.
19. Alzu'bi, A.A.; Alasal, S.I.A.; Watzlaf, V.J. A simulation study of coronavirus as an epidemic disease using agent-based modeling. *Perspect. Health Inf. Manag.* **2021**, *18*, 1g. [PubMed]
20. Chang, S.; Pierson, E.; Koh, P.W.; Gerardin, J.; Redbird, B.; Grusky, D.; Leskovec, J. Mobility network models of COVID-19 explain inequities and inform reopening. *Nature* **2021**, *589*, 82–87. [CrossRef] [PubMed]
21. Nian, G.; Peng, B.; Sun, D.; Ma, W.; Peng, B.; Huang, T. Impact of COVID-19 on urban mobility during post-epidemic period in megacities: From the perspectives of taxi travel and social vitality. *Sustainability* **2020**, *12*, 7954. [CrossRef]
22. Li, Q.; Bessell, L.; Xiao, X.; Fan, C.; Gao, X.; Mostafavi, A. Disparate patterns of movements and visits to points of interest located in urban hotspots across US metropolitan cities during COVID-19. *R. Soc. Open Sci.* **2021**, *8*, 201209. [CrossRef] [PubMed]
23. Newman, M.E. Spread of epidemic disease on networks. *Phys. Rev. E* **2002**, *66*, 016128. [CrossRef] [PubMed]
24. Pastor-Satorras, R.; Castellano, C.; Van Mieghem, P.; Vespignani, A. Epidemic processes in complex networks. *Rev. Mod. Phys.* **2015**, *87*, 925. [CrossRef]
25. Tako, A.A.; Robinson, S. Comparing discrete-event simulation and system dynamics: Users' perceptions. In *System Dynamics*; Springer: Berlin, Germany, 2018; pp. 261–299.
26. Ward, H.; Cooke, G.; Atchison, C.J.; Whitaker, M.; Elliott, J.; Moshe, M.; Brown, J.C.; Flower, B.; Daunt, A.; Ainslie, K.E.; et al. Declining prevalence of antibody positivity to SARS-CoV-2: A community study of 365,000 adults. *MedRxiv* **2020**. [CrossRef]
27. Gudbjartsson, D.F.; Norddahl, G.L.; Melsted, P.; Gunnarsdottir, K.; Holm, H.; Eythorsson, E.; Arnthorsson, A.O.; Helgason, D.; Bjarnadottir, K.; Ingvarsson, R.F.; et al. Humoral immune response to SARS-CoV-2 in Iceland. *N. Engl. J. Med.* **2020**, *383*, 1724–1734. [CrossRef] [PubMed]
28. Zuo, J.; Dowell, A.; Pearce, H.; Verma, K.; Long, H.; Begum, J.; Aiano, F.; Amin-Chowdhury, Z.; Hallis, B.; Stapley, L.; et al. Robust SARS-CoV-2-specific T-cell immunity is maintained at 6 months following primary infection. *Nature Immunol.* **2021**, *22*, 620–626. [CrossRef]
29. Zayet, S.; Royer, P.Y.; Toko, L.; Pierron, A.; Gendrin, V.; Klopfenstein, T. Recurrence of COVID-19 after recovery? A case series in health care workers, France. *Microbes Infect.* **2021**, *23*, 104803. [CrossRef]
30. Kasereka, S.K.; Zohinga, G.N.; Kiketa, V.M.; Ngoie, R.B.M.; Mputu, E.K.; Kasoro, N.M.; Kyandoghere, K. Equation-Based Modeling vs. Agent-Based Modeling with Applications to the Spread of COVID-19 Outbreak. *Mathematics* **2023**, *11*, 253. [CrossRef]
31. De Oliveira, L.B.; Camponogara, E. Multi-agent model predictive control of signaling split in urban traffic networks. *Transp. Res. Part C Emerg. Technol.* **2010**, *18*, 120–139. [CrossRef]
32. Hackl, J.; Dubernet, T. Epidemic spreading in urban areas using agent-based transportation models. *Future Internet* **2019**, *11*, 92. [CrossRef]
33. Nadini, M.; Zino, L.; Rizzo, A.; Porfiri, M. A multi-agent model to study epidemic spreading and vaccination strategies in an urban-like environment. *Appl. Netw. Sci.* **2020**, *5*, 1–30. [CrossRef]
34. Girardi, P.; Gaetan, C. An SEIR Model with Time-Varying Coefficients for Analyzing the SARS-CoV-2 Epidemic. *Risk Anal.* **2021**, *43*, 144–155. [CrossRef]
35. Yin, K.; Mondal, A.; Ndeffo-Mbah, M.; Banerjee, P.; Huang, Q.; Gurarie, D. Bayesian Inference for COVID-19 Transmission Dynamics in India Using a Modified SEIR Model. *Mathematics* **2022**, *10*, 4037. [CrossRef]
36. Zhuge, C.; Shao, C.; Wei, B. An agent-based spatial urban social network generator: A case study of Beijing, China. *J. Comput. Sci.* **2018**, *29*, 46–58. [CrossRef]
37. Jones, N.R.; Qureshi, Z.U.; Temple, R.J.; Larwood, J.P.; Greenhalgh, T.; Bourouiba, L. Two metres or one: What is the evidence for physical distancing in covid-19? *BMJ* **2020**, *370*, m3223. [CrossRef] [PubMed]
38. Lauer, S.A.; Grantz, K.H.; Bi, Q.; Jones, F.K.; Zheng, Q.; Meredith, H.R.; Azman, A.S.; Reich, N.G.; Lessler, J. The incubation period of coronavirus disease 2019 (COVID-19) from publicly reported confirmed cases: Estimation and application. *Ann. Internal Med.* **2020**, *172*, 577–582. [CrossRef] [PubMed]
39. Li, Q.; Guan, X.; Wu, P.; Wang, X.; Zhou, L.; Tong, Y.; Ren, R.; Leung, K.S.; Lau, E.H.; Wong, J.Y.; et al. Early transmission dynamics in Wuhan, China, of novel coronavirus–infected pneumonia. *N. Engl. J. Med.* **2020**, *382*, 1199–1207. [CrossRef]
40. Eurosurveillance Editorial Team. Updated rapid risk assessment from ECDC on the novel coronavirus disease 2019 (COVID-19) pandemic: Increased transmission in the EU/EEA and the UK. *Euro Surveill. Bull. Eur. Sur Les Mal. Transm. Eur. Commun. Dis. Bull.* **2020**, *25*, 680.
41. Mission, W.C.J. *Report of the WHO-China Joint Mission on Coronavirus Disease 2019 (COVID-19)*; WHO: Geneva, Switzerland, 2020.

42. Linton, N.M.; Kobayashi, T.; Yang, Y.; Hayashi, K.; Akhmetzhanov, A.R.; Jung, S.M.; Yuan, B.; Kinoshita, R.; Nishiura, H. Incubation period and other epidemiological characteristics of 2019 novel coronavirus infections with right truncation: A statistical analysis of publicly available case data. *J. Clin. Med.* **2020**, *9*, 538. [CrossRef]
43. Wang, C.; Horby, P.W.; Hayden, F.G.; Gao, G.F. A novel coronavirus outbreak of global health concern. *Lancet* **2020**, *395*, 470–473. [CrossRef]
44. Barabási, A.L.; Pósfai, M. *Network Science*; Cambridge University Press: Cambridge, MA, USA, 2016.
45. Clauset, A.; Shalizi, C.R.; Newman, M.E. Power-law distributions in empirical data. *SIAM Rev.* **2009**, *51*, 661–703. [CrossRef]
46. Dunham, J.B. An agent-based spatially explicit epidemiological model in MASON. *J. Artif. Soc. Soc. Simul.* **2005**, *9*, 690.
47. Topirceanu, A.; Udrescu, M. Statistical fidelity: A tool to quantify the similarity between multi-variable entities with application in complex networks. *Int. J. Comput. Math.* **2017**, *94*, 1787–1805. [CrossRef]
48. Kantner, M.; Koprucki, T. Beyond just "flattening the curve": Optimal control of epidemics with purely non-pharmaceutical interventions. *J. Math. Ind.* **2020**, *10*, 1–23. [CrossRef]
49. Topîrceanu, A.; Udrescu, M.; Udrescu, L.; Ardelean, C.; Dan, R.; Reisz, D.; Mihaicuta, S. SAS score: Targeting high-specificity for efficient population-wide monitoring of obstructive sleep apnea. *PLoS ONE* **2018**, *13*, e0202042. [CrossRef] [PubMed]
50. Udrescu, L.; Bogdan, P.; Chiş, A.; Sîrbu, I.O.; Topîrceanu, A.; Văruţ, R.M.; Udrescu, M. Uncovering New Drug Properties in Target-Based Drug–Drug Similarity Networks. *Pharmaceutics* **2020**, *12*, 879. [CrossRef]
51. Saadat, S.; Rawtani, D.; Hussain, C.M. Environmental perspective of COVID-19. *Sci. Total Environ.* **2020**, *728*, 138870. [CrossRef] [PubMed]
52. Rypdal, K.; Bianchi, F.M.; Rypdal, M. Intervention fatigue is the primary cause of strong secondary waves in the COVID-19 pandemic. *Int. J. Environ. Res. Public Health* **2020**, *17*, 9592. [CrossRef]
53. Mei, S.; Chen, B.; Zhu, Y.; Lees, M.H.; Boukhanovsky, A.; Sloot, P.M. Simulating city-level airborne infectious diseases. *Comput. Environ. Urban Syst.* **2015**, *51*, 97–105. [CrossRef]
54. Mao, L.; Bian, L. Spatial–temporal transmission of influenza and its health risks in an urbanized area. *Comput. Environ. Urban Syst.* **2010**, *34*, 204–215. [CrossRef]
55. Luo, W.; Gao, P.; Cassels, S. A large-scale location-based social network to understanding the impact of human geo-social interaction patterns on vaccination strategies in an urbanized area. *Comput. Environ. Urban Syst.* **2018**, *72*, 78–87. [CrossRef]
56. Topîrceanu, A.; Precup, R.E. A novel geo-hierarchical population mobility model for spatial spreading of resurgent epidemics. *Sci. Rep.* **2021**, *11*, 14341. [CrossRef]
57. Topîrceanu, A. Benchmarking Cost-Effective Opinion Injection Strategies in Complex Networks. *Mathematics* **2022**, *10*, 2067. [CrossRef]
58. Li, W.; Xue, X.; Pan, L.; Lin, T.; Wang, W. Competing spreading dynamics in simplicial complex. *Appl. Math. Comput.* **2022**, *412*, 126595. [CrossRef]
59. Topîrceanu, A. Competition-Based Benchmarking of Influence Ranking Methods in Social Networks. *Complexity* **2018**, *2018*, 4562609. [CrossRef]
60. Pastor-Satorras, R.; Vespignani, A. Immunization of complex networks. *Phys. Rev. E* **2002**, *65*, 036104. [CrossRef] [PubMed]
61. Topîrceanu, A. Immunization using a heterogeneous geo-spatial population model: A qualitative perspective on COVID-19 vaccination strategies. *Procedia Comput. Sci.* **2021**, *192*, 2095–2104. [CrossRef]
62. Matrajt, L.; Leung, T. Evaluating the effectiveness of social distancing interventions to delay or flatten the epidemic curve of coronavirus disease. *Emerg. Infect. Diseases* **2020**, *26*, 1740. [CrossRef]
63. European Centre for Disease Prevention and Control (An agency of the European Union). Data on the Daily Number of New Reported COVID-19 Cases and Deaths by EU/EEA country. Available online: https://www.ecdc.europa.eu/en/covid-19/data (accessed on 27 October 2022).